J. Fluid Mech. (1968), *vol.* 31, *part* 2, *pp.* 343–360
Printed in Great Britain

Penetrative convection

By STEVEN MUSMAN

High Altitude Observatory, Boulder, Colorado,
and Goddard Institute for Space Studies, NASA, New York, New York†

(Received 30 March 1967)

A penetrative convection problem which depends on the density maximum of water near 4 °C is solved numerically. When a layer of water has its lower boundary maintained at 0 °C and its upper boundary at some temperature above 4 °C, the layer will be divided into a lower convectively unstable region and an upper convectively stable region. Steady-state finite-amplitude solutions to this problem are obtained using the mean field approximation and free boundaries.

Convective mixing alters the temperature structure of the layer so that the temperature of a large fraction of the layer is slightly below the temperature of maximum density, in agreement with laboratory measurements. The largest motions are found in a principal convective cell which extends from the lower boundary to a temperature of 7° or 8 °C. Above the principal cell one or more counter cells may form, depending on the temperature of the upper boundary. The velocities in the counter cells are substantially less than those in the principal cell and fall off rapidly going upward. When the temperature of the upper boundary is 7 °C or higher, convection first takes place at a finite amplitude and at a Rayleigh number less than that predicted by the linear theory. When the temperature of the upper boundary is 10 °C or higher, the upper boundary is no longer important dynamically to the system.

As the Rayleigh number is increased above critical stability the velocities in the principal cell, heat transport and the distortion of the temperature field all increase. In addition, the principal cell becomes more slender and fills a greater fraction of the layer. Also, as the Rayleigh number increases the counter cells become more flattened, fill a smaller fraction of the layer, and the velocities in the counter cells decrease relative to those in the principal cell.

The most important penetration of convective motions takes place in the form of nearly horizontal motions in the lowest part of the stable region, corresponding to the upper part of the principal cell. The velocities of these motions are a large fraction of the largest vertical velocities in the unstable region.

1. Introduction

There are several cases in geophysics and astrophysics where the penetration of convective motions into an overlying convectively stable region is important. One such case is the observable motions in the outer stable regions of the

† Present address: Sacramento Peak Observatory Sunspot, New Mexico.

sun (summarized by Leighton 1963). These motions presumably arise from the solar convective zone which is just below them. Another case is the dynamics of cumulus clouds studied by Simpson, Simpson, Andrews & Eaton (1965).

Malkus (1960) proposed the following method for studying penetrative convection in the laboratory: the lower boundary of a layer of water is maintained at a temperature of 0 °C and the upper boundary at a temperature higher than 4 °C. The region below the density maximum of water near 4 °C is convectively unstable, while the region above the density maximum is convectively stable. Convective motions occurring in the lower unstable region may penetrate into the upper stable region. This experiment has been performed in the laboratory by Furumoto & Rooth (1961) and Townsend (1964). It has also been discussed theoretically by Veronis (1963).

In ordinary parallel plate convective experiments (such as Globe & Dropkin 1959) the material boundaries of the laboratory container strongly influence the motions of the convecting fluid. The largest changes take place in thin layers near the boundaries, and the form of the heat transport law may be predicted from a scale analysis which does not include the thickness of the layer. In the ice-water problem the extent that the convective motions penetrate into the upper stable region does not depend on the upper boundary when the stable region is sufficiently thick. This feature of the ice-water experiment makes it useful for studying situations where no solid boundary exists.

Steady-state solutions to this problem will be found numerically using free boundaries and the mean field approximation (Herring 1963), which includes certain nonlinear terms but neglects nonlinear terms generally associated with turbulence. These solutions will be compared with laboratory results and the effect of the approximations used will be discussed.

2. Derivation of equations

The basic dynamical equations of the problem are the Navier–Stokes equation

$$\frac{\partial \mathbf{V}}{\partial t} + (\mathbf{V}.\boldsymbol{\nabla})\,\mathbf{V} = -\frac{1}{\rho}\boldsymbol{\nabla}\,\delta p - \frac{g}{\rho}\,\delta\rho\,\hat{k} + \nu\nabla^2\mathbf{V}, \tag{1}$$

the continuity equation

$$\boldsymbol{\nabla}.\mathbf{V} = 0, \tag{2}$$

and the heat equation

$$\frac{\partial T}{\partial t} + \mathbf{V}.\boldsymbol{\nabla}T = \kappa\nabla^2 T. \tag{3}$$

Equations (1), (2), (3) are written for an incompressible fluid of mean density $\bar{\rho}$ where v is the velocity vector, g is the acceleration of gravity, $\hat{k}$ is a unit vector in the vertical direction, ν is the dynamical viscosity, T is the temperature, and κ is the thermometric conductivity. Hydrostatic pressure and density have been removed from (1), leaving only the changes in pressure and density δp, $\delta\rho$ associated with the motion. The Boussinesq approximation is assumed; i.e. changes in density, $\delta\rho$, are considered to be a function of temperature alone

and taken into account only in the buoyancy term. It is convenient to transform equations (1), (2), (3) into

$$\left(\nu\nabla^2 - \frac{\partial}{\partial t}\right)\nabla^2 w + \{\boldsymbol{\nabla}\times\boldsymbol{\nabla}\times(\mathbf{V}.\boldsymbol{\nabla})\,\mathbf{V}\}_z = \frac{g}{\rho}\nabla_1^2\,\delta\rho, \tag{4}$$

$$\frac{\partial\overline{T}'}{\partial t} + \frac{d}{dz}(\overline{WT'}) = \kappa\frac{d^2\overline{T}}{dz}, \tag{5}$$

$$\frac{\partial T'}{\partial t} + w\frac{\partial\overline{T}}{\partial z} + \{\mathbf{V}.\boldsymbol{\nabla}T' - \overline{\mathbf{V}.\boldsymbol{\nabla}T'}\} = \kappa\nabla^2 T', \tag{6}$$

where w is the vertical component of the velocity and the operator ∇_1^2 is the horizontal Laplacian operator $(\partial^2/\partial x^2)+(\partial^2/\partial y^2)$. Equation (4) is obtained by operating on (2) twice with the curl operator and taking the vertical component. Equations (5) and (6) have been derived from (3) together with the substitution

$$T(x,y,z,t) = \overline{T}(z,t) + T'(x,y,z,t), \tag{7}$$

which divides the temperature field into a mean component $\overline{T}$ and a fluctuating component T'. When (7) is substituted into (3) and the horizontal average taken, denoted by a horizontal bar, equation (5) results. Subtracting (5) from (3) yields equation (6). The dependent variables in the system of equations (4)–(6) may be divided into mean quantities with non-zero horizontal averages and fluctuating quantities whose horizontal average is zero. $\overline{T}$ is a mean quantity, while T' and all components of the velocity are fluctuating quantities. In the mean field approximation (see Herring 1963) nonlinear interactions between mean and fluctuating quantities are taken into account, while nonlinear interactions between fluctuating quantities are ignored. The terms in brackets in (4) and (6) are fluctuating interactions.

Free, conducting boundaries will be used at the bottom and the top of the layer,

$$w,\ \frac{\partial^2 w}{\partial z^2},\ T' = 0 \quad \text{at} \quad z = 0, h, \tag{8}$$

where z is the vertical co-ordinate and h is the thickness of the layer. The bottom boundary will be maintained at 0 °C and the upper boundary at a higher temperature

$$\overline{T} = 0 \quad \text{at} \quad z = 0; \qquad T = \lambda\Delta T \quad \text{at} \quad z = h, \tag{9}$$

where ΔT is the difference between 0 °C and the temperature of maximum density near 4 °C and λ is a parameter designating the temperature of the upper boundary. The equation of state of ice water will be taken as

$$\rho = \bar{\rho}[1 - \alpha(T - T_0)^2], \tag{10}$$

where $T_0 = 3{\cdot}98$ °C and $\alpha = 8{\cdot}0\times10^{-6}/(\text{degC})^2$. Equation (10) fits the measured density of ice water within 4 % between 0° and 8 °C and is off by 20 % at 24 °C. The buoyancy term on the right-hand side of equation (4) may be expanded with the help of equations (7) and (10) into

$$\frac{g}{\bar{\rho}}\nabla_1^2\delta\rho = -\frac{2\alpha g}{\bar{\rho}}[(\overline{T} - T_0)\nabla_1^2 T' + \tfrac{1}{2}\nabla_1^2 T'^2]. \tag{11}$$

The second term on the right-hand side of equation (11) is a fluctuating interaction and will be subsequently neglected. The dimensionless number describing the degree of convective instability, the Rayleigh number, will be defined as follows:

$$R = \frac{1}{\pi^4} \frac{gl^3}{\kappa\nu} \frac{\Delta\rho}{\bar{\rho}}, \tag{12}$$

where $\Delta\rho$ is the difference in density in the unstable portion of the layer and l is the height of the unstable portion of the layer. Equation (12) differs from the conventional definition by a factor of π^4. In evaluating the Rayleigh number the following relationships are useful:

$$\left.\begin{aligned} l = h, \quad & \frac{\Delta\rho}{\rho} = (2\lambda - \lambda^2)\,\alpha\Delta T^2 \quad \text{for} \quad 0 \leqslant \lambda \leqslant 1, \\ l = \frac{h}{\lambda}, \quad & \frac{\Delta\rho}{\bar{\rho}} = \alpha\Delta T^2 \quad \text{for} \quad \lambda \geqslant 1. \end{aligned}\right\} \tag{13}$$

When (4) is non-dimensionalized using h/π, $h/\pi^2\kappa$ and $\lambda\Delta T/\pi$ for units of length, time and temperature the following results:

$$\left(\nabla^2 - \frac{1}{\sigma}\frac{\partial}{\partial t}\right)\nabla^2 w + \frac{1}{\sigma}\{\nabla \times \nabla \times (V.\nabla)\,V\}_z = -F(\lambda)\,R\left\{\left[-1 + \frac{\lambda}{\pi}(z+\psi)\right]\nabla_1^2\theta + \frac{\lambda}{2\pi}\nabla_1^2\theta^2\right\}. \tag{14}$$

$F(\lambda)$ is defined by

$$\left.\begin{aligned} F(\lambda) &= \frac{1}{1 - \frac{1}{2}\lambda} \quad (0 \leqslant \lambda \leqslant 1); \\ F(\lambda) &= 2\lambda^4 \quad (\lambda \geqslant 1); \end{aligned}\right\} \tag{15}$$

where θ is the non-dimensional form of T and σ is the Prandtl number, the quantity in brackets multiplying $\nabla_1^2\,\theta$ corresponds to $(\bar{T} - T_0)$, and ψ, a function of z and t, represents the departure of the mean temperature profile from a straight line. Steady-state solutions will be found of the form

$$w = f(x, y)\,W(z), \tag{16}$$

$$\theta = f(x, y)\,\Theta(z). \tag{17}$$

The function f has the following properties:

$$\nabla_1^2 f = -s^2 f, \tag{18}$$

$$\bar{f} = 0, \tag{19}$$

$$\bar{f}^2 = 1, \tag{20}$$

where s is a normalized horizontal wave-number. Solutions chosen in this manner have a regular horizontal form. Specific expressions for f have been worked out for various types of cells, such as a convective roll, square cell, hexagonal cell, or cylindrical cell. For a convective roll

$$f = \sqrt{2}\sin sx. \tag{21}$$

The horizontal and vertical components of the velocity for this case are:

$$u = \frac{\sqrt{2}}{s}\cos sx\frac{dW(z)}{dz}, \tag{22}$$

$$w = \sqrt{2}\sin sx\, W(z). \tag{23}$$

Equations (14) and (6) become for the convective roll

$$(\sqrt{2}\sin sx)\left(\frac{d^2}{dz^2}-s^2\right)W(z)+\frac{1}{\sigma}\left(\frac{2}{s}\cos 2sx\right)\left(W\frac{d^3W}{dz^3}-\frac{dW}{dz}\frac{d^2W}{dz^2}\right)$$
$$= -F(\lambda)Rs^2\left\{(\sqrt{2}\sin sx)\left[-1+\frac{\lambda}{\pi}(z+\psi)\right]\Theta+\frac{\lambda}{\pi}(4s^2\cos 2sx)\Theta^2\right\}, \tag{24}$$

$$(\sqrt{2}\sin sx)\left(1+\frac{d\psi}{dz}\right)W(z)+(\cos 2sx)\left(\frac{dW}{dz}\Theta-W\frac{d\Theta}{dz}\right)=(\sqrt{2}\sin sx)\left(\frac{d^2}{dz^2}-s^2\right)\Theta. \tag{25}$$

Equations (24) and (25) will be used to estimate the effect of ignoring the fluctuating interactions. The three fluctuating interactions in equations (24) and (25) all contain the factor $\cos 2sx$ and arise from the coupling of the fundamental horizontal mode into the next higher horizontal mode which is ignored by assuming (18). Equations (24) and (25) cannot be used to deal with the fluctuating interactions in a self-consistent manner as the coupling of the next higher horizontal mode into the fundamental mode is ignored.

The final set of equations to be solved which neglects fluctuating interactions is

$$\left(\frac{d^2}{dz^2}-s^2\right)W = D, \tag{26}$$

$$\left(\frac{d^2}{dz^2}-s^2\right)D = F(\lambda)Rs^2\left[-1+\frac{\lambda}{\pi}(z+\psi)\right]\Theta, \tag{27}$$

$$\frac{d^2\psi}{dz^2} = \frac{d}{dz}(W\Theta), \tag{28}$$

$$\left(\frac{d^2}{dz^2}-s^2\right)\Theta = \left(1+\frac{d\psi}{dz}\right)W, \tag{29}$$

with boundary conditions

$$W, D, \psi, \Theta = 0 \quad \text{at} \quad z = 0, \pi. \tag{30}$$

Equations (26) and (27) are derived from equation (14) with the addition of the auxiliary variable D which is defined in equation (26).

The system of equations (26)–(29) is a system of ordinary differential equations obtained from the system of partial differential equations (1)–(3). If the velocity and temperature fields are thought of in terms of normal modes, only one mode has been included in the horizontal, while a large number of modes have been included in the vertical (in practice limited by the integration step size). Useful results can be obtained in this manner since the largest changes take place in thin layers near the upper and lower boundaries. The system of equations (26)–(29) reduces to those solved by Herring (1963) when $\lambda = 0$ and the signs of the

temperature variables ψ, Θ are changed. The choice of signs for temperature quantities is related to the fact that the fluid rising from the bottom boundary in the ice-water problem is colder than its surroundings while the opposite is true in ordinary convective problems. Equation (28) is exact and expresses the fact that the divergence of the total flux vanishes. Its integral,

$$N = 1 + \frac{d\psi}{dz} - W\Theta, \tag{31}$$

states that the total horizontally averaged flux N, expressed in units of the flux which would be conducted between the two boundaries without convection (the Nusselt number), is conserved at all levels. The first two terms on the right-hand side of (31) are the conductive flux and the third is the convective flux. Equations (24), (27) and (29), with the omission of ψ, are the linearized stability equations of the problem, which have been solved by Veronis (1963).

The system of equations (26)–(29) forms an eighth-order system of nonlinear ordinary differential equations with boundary conditions given at two different points. The solution is obtained by an iterative technique. First an approximate solution is chosen, substituted into the original equations, and the residuals are computed. Then the equations are linearized about the approximate solution and a system of linear equations is solved to find the corrections to the original solution which could eliminate the residuals. The corrections or an appropriate fraction of them are added to the original approximation and the process repeated until the corrections become very small. The procedure is essentially the Newton–Raphson technique; described by Fox (1957) as the 'η' method. The procedure also resembles that used by Henyey *et al.* (1959) for constructing stellar models. In practice a very large matrix, with non-zero elements concentrated along a narrow band near the diagonal, must be inverted. This is accomplished by a Gaussian elimination procedure where the form of the equations has been chosen in order to well condition the matrix.

Computations were begun for $\lambda = 0$ and a Rayleigh number just above the critical Rayleigh number. Analytic expressions similar to those derived by Malkus & Veronis (1958) were used as the initial approximations. Several solutions of Herring (1963) were reproduced to check numerical procedures. Then λ and R were increased slowly, using at each step previously converged results for initial approximations. Near $\lambda = 2$ oscillations developed in the iteration with a period of about 25 iteration steps. It is not clear whether these oscillations are numerical or physical. The physical system can oscillate in the form of internal gravity waves. It was necessary to damp out these oscillations by an elaborate and arbitrary procedure in order to obtain convergence.

3. Results and discussion

The nature of the solutions and the finite instability

The calculated mean temperature profile for $\lambda = 6$, $R = 5$, $s = 1{\cdot}7$ is plotted as a solid line in figure 1. If convection did not take place the temperature distribution would be determined by conduction alone, represented by the broken line

in figure 1. Convective motions, when they do occur, tend to bring the temperature distribution closer to the adiabatic one. For an incompressible fluid the adiabatic temperature distribution is a constant temperature. The temperature of most of the layer is just below that of maximum density, and hence just slightly unstable. The dashed line is the laboratory measurement of Townsend (1964). The detailed agreement between theory and observations will be discussed later.

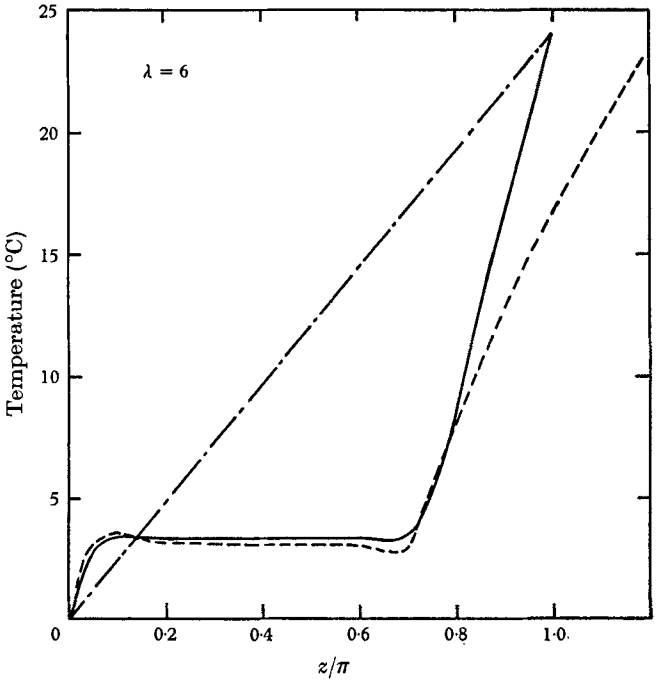

FIGURE 1. Mean temperature profile. —, $\lambda = 6$, $R = 5$, $s = 1{\cdot}7$; — · —, linear, – – –, measurements of Townsend (1964).

The calculated velocity and temperature fields for $\lambda = 6$, $R = 2{\cdot}5$, $s = 1{\cdot}65$ are shown in figure 2. These are represented in terms of the cross-section of a convective roll, although the mean field equations do not distinguish between the various types of horizontal plan forms. The left-hand portion of figure 2 displays contours of equal stream function, which in the steady state are also particle paths. There is one principal cell and two counter cells above it. The vertical motion on the right-hand side of these cells is upward in the principal cell, downward in the first counter cell, and again upward in the second counter cell. The velocities are much smaller in the counter cells than in the principal cell so that it was not possible to plot contours uniformly throughout the entire region. The number in the centre of each cell is the maximum vertical velocity in that cell. The contours plotted are equal fractions of the maximum stream-function for that cell.

Contours of equal temperature are plotted in the right-hand portion of figure 2 for every degree centigrade from 0 at the bottom to 24 at the top. It can be seen by comparing the left- and right-hand portions of figure 2 that the principal

cell penetrates into the stable region. The mean temperature of the top of the principal cell is 7·5 °C, substantially above the temperature of maximum density. The largest horizontal temperature differences are found near the top and bottom of the principal cell. If the nature of the velocity and temperature fields for the principal cell shown in figure 2 are compared with those obtained by Rayleigh (1916) for the case of the marginal convective stability of a layer of an ordinary fluid, it is found that the velocity fields are very similar, while the temperature fields are substantially different. The velocity and temperature fields for the principal cell also closely resemble the results of Herring (1963).

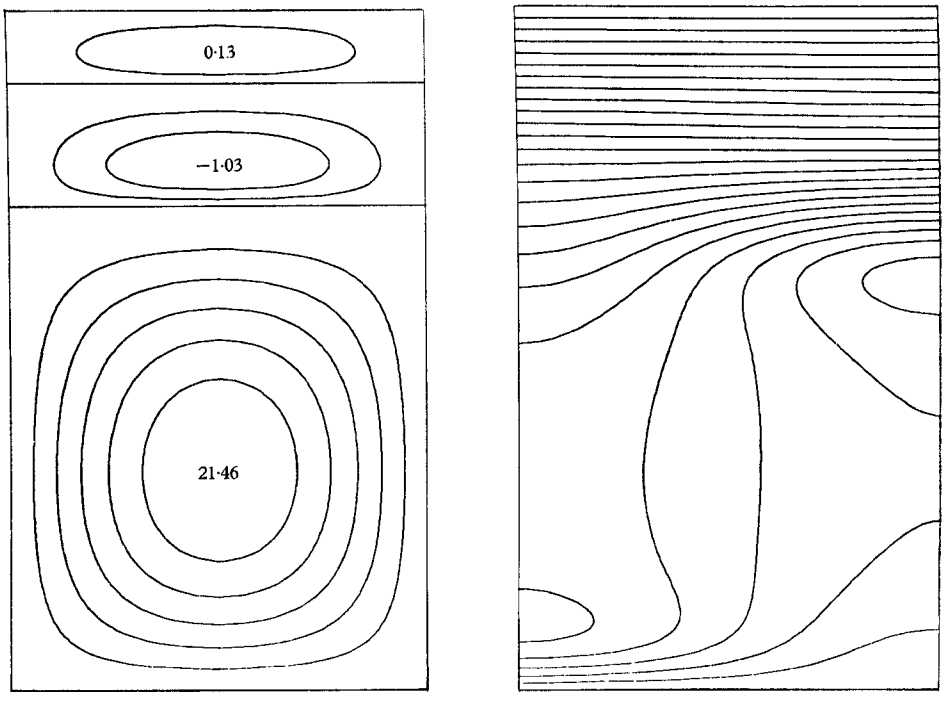

FIGURE 2. Velocity and temperature fields for $\lambda = 6$, $R = 2{\cdot}5$, $s = 1{\cdot}65$. On the left streamlines of the motion with the maximum vertical velocities indicated for each cell. On the right contours of equal temperature for every degree centigrade from 0 at the bottom to 24 at the top.

The normalized horizontal wave-number, s, which for the convective roll is simply the ratio of the thickness of the layer to the width of the cell, is chosen to maximize the heat transport. Figure 3 shows the variation of heat transport with s for $\lambda = 3$. For a given Rayleigh number, R, the Nusselt number is plotted as a solid line against s. This can be compared directly with figure 15 in Herring (1963). The dotted line shows the maximum Nusselt number, N, obtainable for a given R. The point at the centre of the solid curves with parameters $R = 1{\cdot}84$, $s = 1{\cdot}16$ was the lowest R for which a solution was attained. No solutions were obtained below the dashed line in figure 3. The point at $N = 1$ (i.e. no convection) with parameters $R = 2{\cdot}82$, $s = 1{\cdot}52$ is the critical Rayleigh number predicted by the linearized stability theory.

This feature may also be seen in figure 4, where the Nusselt number is plotted against the Rayleigh number for $\lambda = 6$; each point on the solid line of figure 4 gives the maximum Nusselt number at that Rayleigh number (given by a point on the dotted line in figure 3). The critical Rayleigh number for the linearized problem is also represented by a point at $N = 1$ in figure 4. A dashed curve connects this point and the solutions obtained. Attempts to obtain solutions along this dashed

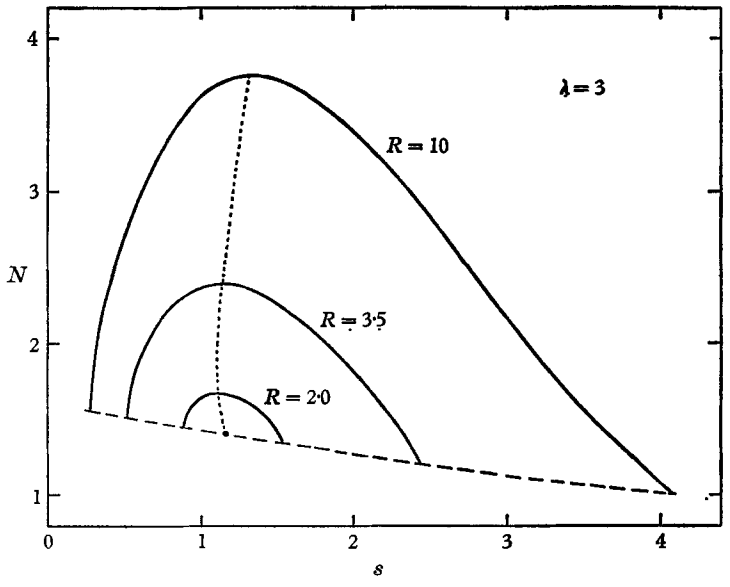

FIGURE 3. Heat transport versus horizontal wave-number.

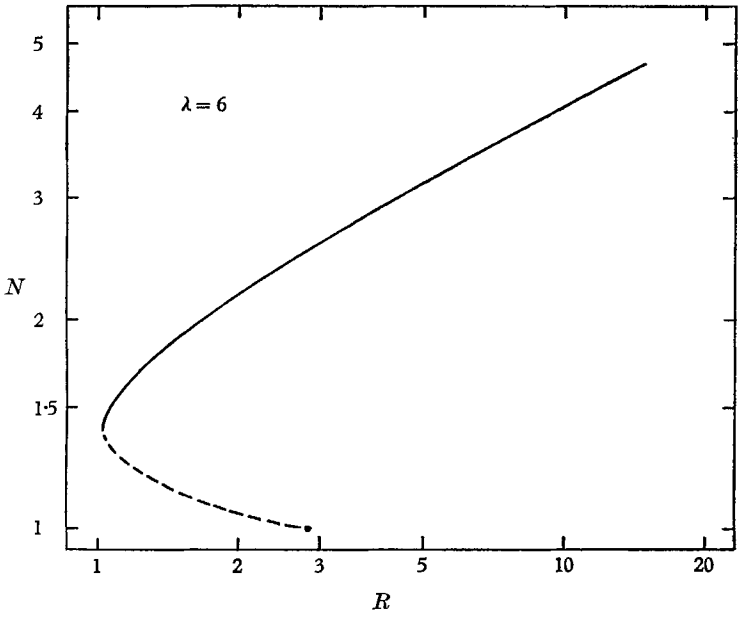

FIGURE 4. Heat transport versus Rayleigh number for $\lambda = 6$.

curve were unsuccessful. All initial approximations used converged either to the trivial solution or to the solution given by the solid line in figure 4. It is likely that, for Rayleigh numbers between the critical Rayleigh number for the linear problem and the minimum Rayleigh number obtained, there are two possible solutions, one small-amplitude and small Nusselt number solution represented by a point on the dashed part of the curve in figure 4 and one large-amplitude and larger Nusselt number solution represented by a point on the solid part of the same curve. The physically realizable (and also numerically stable) solution is the one with the largest heat transport. Convection first takes place at a finite amplitude and at a Rayleigh number below that predicted by the linear theory. Veronis (1963) first demonstrated that the ice-water problem had a finite convective instability and predicted the nature of the curve in figure 4. For a discussion of another example of a finite convective instability see Veronis (1966).

An important feature which the nonlinear theory takes into account and which is omitted by the linear theory is the distortion of the mean temperature profile. For example, compare the solid curve in figure 1 with the broken line. The definition of the Rayleigh number, equation (12), contains the height of the unstable portion of the layer. For the case plotted in figure 1, this distance is 4·3 times as large for the distorted profile as for the linear profile. If a quantity r is defined as the ratio of these two distances, then an effective Rayleigh number R_E, which takes into account the actual height of the unstable layer, can be expressed as

$$R_E = r^3 R. \tag{32}$$

For the case plotted in figure 1, R is 5 and R_E is 406.

The results of both the linear and the nonlinear stability analyses for the ice-water problem are displayed in figure 5. The solid line represents the results of the linear problem, which is an extension of the results given by Veronis (1963). For $\lambda \leqslant 1$, where there is no stable layer, the initial Rayleigh number is always close to the $\lambda = 0$ critical Rayleigh number of $\frac{27}{4}$ ($\frac{27}{4}\pi^4$ in conventional units). The initial sharp drop in Rayleigh number for λ slightly greater than unity results from the fact that a very thin stable layer near the upper boundary is constrained to move nearly horizontally while buoyancy forces can only effect vertical motions. The dotted line plotted in figure 5 has the equation

$$R = 6{\cdot}71/\lambda^3. \tag{33}$$

This would describe the critical Rayleigh number if the critical Rayleigh number were always equal to the critical Rayleigh number at $\lambda = 1$, but the entire thickness of the layer acts as if it were unstable. As λ increases, and the thickness of the stable layer increases relative to the unstable layer, the stable layer is less constrained to move vertically and thus can exert a stabilizing influence on the system so that the critical Rayleigh number becomes further above the dotted line.

When the temperature of the upper boundary is less than about 7 °C, convection first appears at an infinitesimal amplitude, and the critical Rayleigh number is that given by the linear theory. However, as λ increases above this level, con-

vection first appears at a finite amplitude at a lower Rayleigh number than that given by the linear theory. The critical Rayleigh number given by the nonlinear theory is plotted in figure 5 as the lower dashed curve. The critical effective Rayleigh number is plotted as the upper dashed curve. Since the difference between these curves is a measure of the distortion of the mean temperature profile, it is apparent that the distortion of the mean temperature profile at marginal stability increases as λ increases. The difference between the critical

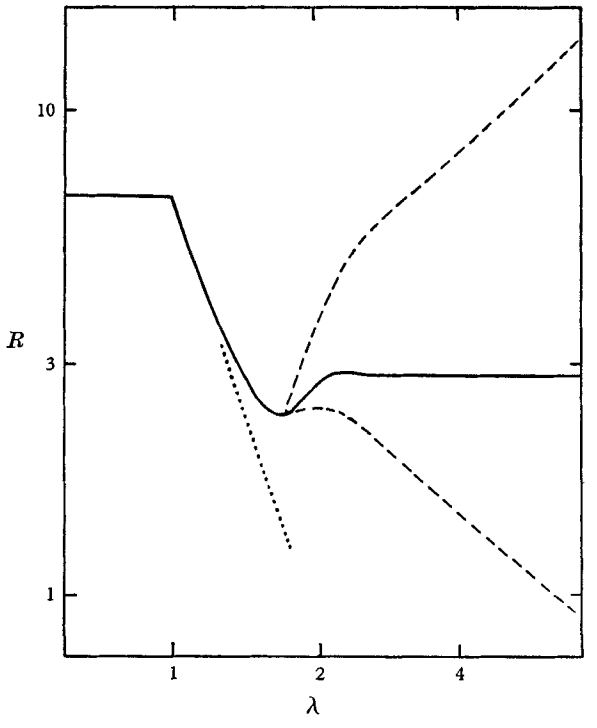

FIGURE 5. Linear and nonlinear stability. —, critical Rayleigh number for linear theory; – – –, nonlinear results: critical Rayleigh number (lower curve) and critical effective Rayleigh number (upper curve).

Rayleigh number predicted by the linear theory and that predicted by the nonlinear theory is probably related to the fact that the linear theory omits the distortion of the mean temperature profile. It is not possible to characterize either the critical R or R_E for the nonlinear case by a single number. For λ greater than 2·5 the Nusselt number is always near 1·4 at marginal stability and decreases very slowly for λ greater than 4.

The influence of λ and R

The concept of an effective Rayleigh number, equation (32), is useful in comparing results for different λ. Figure 6 displays velocity and temperature fields $\lambda = 3$, $R = 10$, $s = 1{\cdot}35$ in a manner similar to figure 2. The two cases have the same effective Rayleigh number but different upper boundary temperature. In physi-

cal terms both have the same distance between the bottom boundary and the height of maximum density, since all other quantities defining the Rayleigh number, equation (12), are either physical or mathematical constants. Figures 2 and 6 have been constructed with this distance the same for both. The mean temperature profile between 0 and 12 °C is almost the same for both cases. In addition an effective Nusselt number defined in a manner similar to the effective Rayleigh number,

$$N_E = rN, \tag{34}$$

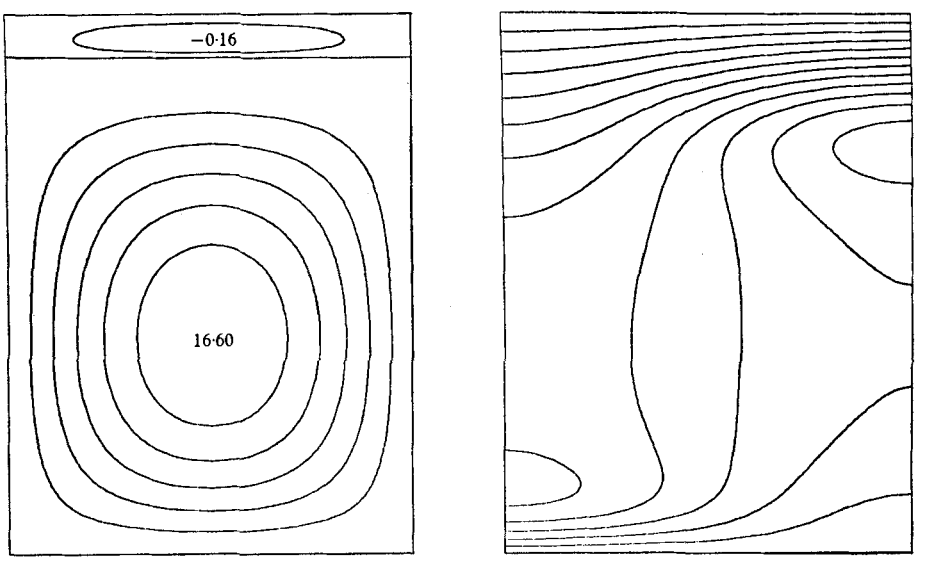

FIGURE 6. Velocity and temperature fields for $\lambda = 3$, $R = 10$, $s = 1{\cdot}35$.

is the same for both cases. The maximum vertical velocity in the principal cell, when expressed in physical units, is nearly the same for figures 2 and 6. However, the velocity and horizontal temperature fields are slightly different, as they must be since the upper boundary conditions are different in the two cases. When other cases are examined which have the same R_E but different λ, it can be concluded that the nature of the principal cell is determined by R_E alone and is independent of the temperature of the upper boundary as long as the upper boundary is sufficiently high.

The number of counter cells depends on the amount of stable layer available. When λ is 2 or less no counter cells form. When λ is between 2·2 and 4 one counter cell is present. For a λ of 5 or 6 there are two counter cells. If $\lambda = 7$ the stable layer contains three counter cells. These cells are not important to the system dynamically. The motions and temperature differences in the counter cells are much smaller than those in the principal cell and result from the fact that the motion in an incompressible fluid will fill the entire available region.

A curve of N_E, defined in (34), versus R_E, defined in (32), is plotted in figure 7. This curve has a similar form to the plot of Nusselt number versus Rayleigh number for laboratory results in figure 5 of Silveston (1958). The cases shown in

figures 2 and 6 are both represented by the point $N_E = 9{\cdot}1$, $R_E = 138$ in figure 7. The location of critical stability for various λ's are also indicated (compare with the upper dashed curve in figure 5). For λ less than 2·5 the curve in figure 7 refers only to critical stability. When the stable portion of the layer is this narrow, the upper boundary is still important in determining the heat flux. Results for λ less than 2·5 but R_E greater than the critical value lie near but not on the curve in figure 7. For λ greater than or equal to 2·5 this curve represents the effective

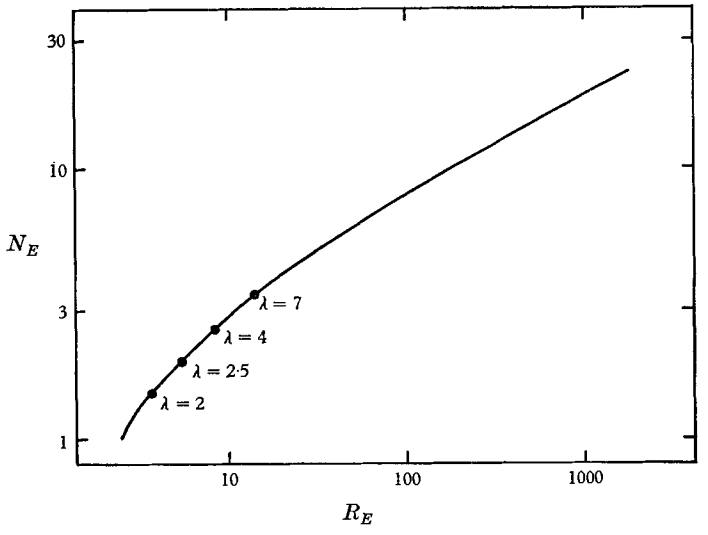

FIGURE 7. Effective heat transport versus effective Rayleigh number.

heat flux for all λ's for which the system is convectively unstable at that particular effective Rayleigh number. Thus, once the upper boundary is at least 10 °C, the nature of the principal cell is determined by the effective Rayleigh number, and hence the heat transport is also determined as the motions and temperature differences in the counter cells are too small to contribute significantly to the transport. The point at which the upper boundary becomes unimportant in determining the heat transport is also the point at which the first counter cell is just beginning to form, and it seems that the formation of at least one counter cell is essential in isolating the principal cell from the upper boundary.

The effect of varying the Rayleigh number will now be examined. Figure 8 shows the velocity and temperature fields for $\lambda = 6$, $R = 1{\cdot}017$, $s = 1{\cdot}72$. This is the critical Rayleigh number for an upper boundary temperature of 24 °C; no smaller-amplitude motions are possible. Figure 8 may be compared directly with figure 2, which shows conditions for the same upper boundary temperature but at a higher Rayleigh number. As the Rayleigh number is increased the velocities in the principal cell become larger, the temperature field is more distorted, and the heat transport increases. This effect can be further seen in figure 9, which presents the velocity and temperature fields for $\lambda = 6$, $R = 12$, $s = 1{\cdot}85$. The effective Rayleigh numbers for figures 8, 2 and 9 are respectively that of

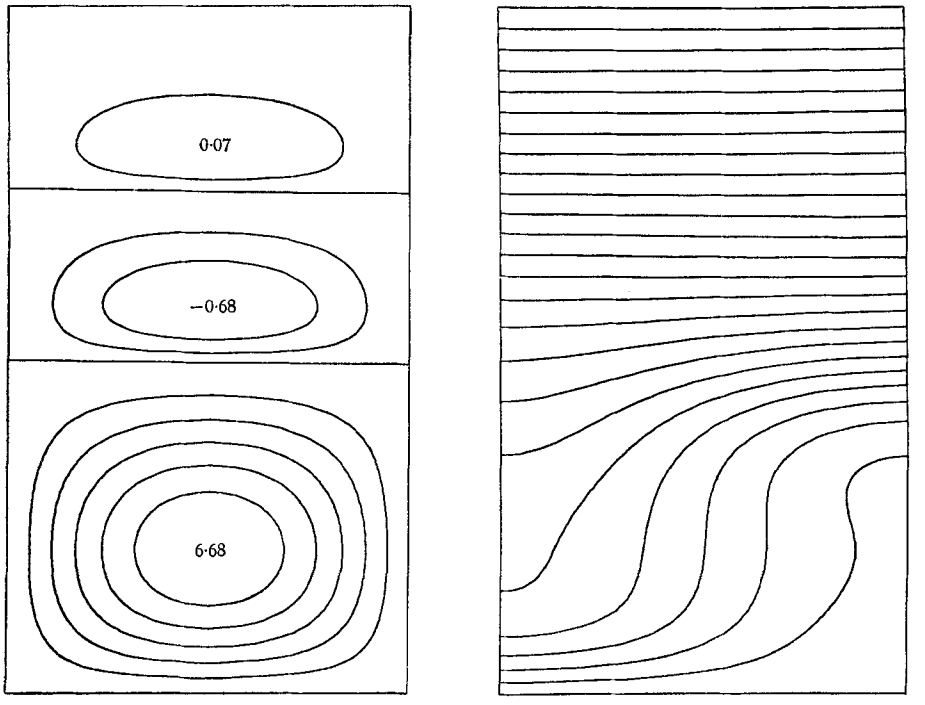

FIGURE 8. Velocity and temperature fields for $\lambda = 6$, $R = 1{\cdot}017$, $s = 1{\cdot}72$.

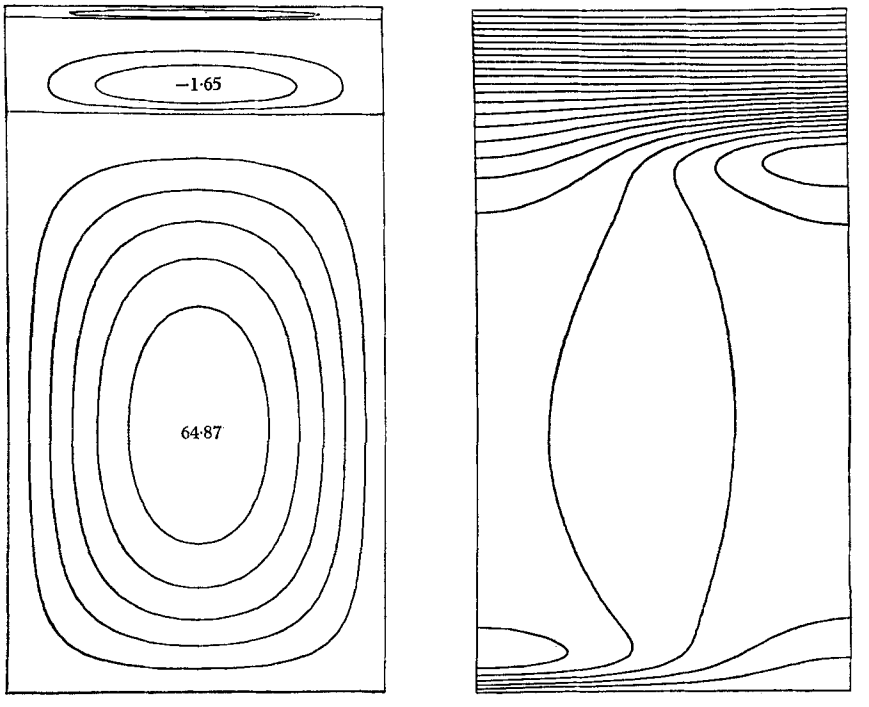

FIGURE 9. Velocity and temperature fields for $\lambda = 6$, $R = 12$, $s = 1{\cdot}85$.

critical stability and roughly 10 and 100 times critical stability. Comparing these three figures gives a good general picture of the effect of varying the Rayleigh number on the ice-water system.

The normalized horizontal wave-number, s, is not very sensitive to the Rayleigh number. Thus for a convective roll the ratio of the height of the layer to the width of the cell does not change much for a given λ. However, the fraction of the layer occupied by the principal cell increases rapidly with increasing Rayleigh number. For the cases presented in figures 8, 2 and 9 the principal cell occupies respectively 48, 71 and 85 % of the layer. Thus if a quantity s', similar to s, is defined with respect to the principal cell alone it would increase monotonically with increasing Rayleigh number. For a convective roll s' is the height to width ratio of the principal cell. The values of s' for the cases illustrated in figures 8, 2 and 9 are 0·65, 1·04 and 1·48. Also s' depends only on R_E for all λ greater than 2·5. The value of s' at critical stability in figure 8 is close to that of 0·71 obtained by Rayleigh (1916) for the critical stability of the ordinary parallel plate convection problem.

As the shape of the principal cell becomes more elongated with increasing Rayleigh number, the shape of the counter cells becomes more flattened. The velocities in the counter cells become smaller compared with the velocities in the principal cell. The maximum vertical velocities for the three cells in the case illustrated in figure 8 are in the ratio $1:1{\cdot}0\times10^{-1}:1{\cdot}1\times10^{-2}$. The same ratios for the cases shown in figures 2 and 9 are

$$1:4{\cdot}8\times10^{-2}:5{\cdot}9\times10^{-3} \quad \text{and} \quad 1:2{\cdot}6\times10^{-2}:9{\cdot}1\times10^{-6}.$$

For Rayleigh numbers larger than that shown in figure 9, the second counter cell disappears (or at least becomes smaller than the integration step size).

The temperature at the top of the principal cell is a measure of the penetration of the motions into the stable layer. This quantity increases only slightly with increasing Rayleigh number. The temperatures at the top of the principal cell for the three cases illustrated in figures 8, 2 and 9 are respectively 6·8°, 7·5° and 8·0 °C. The difference in density between the maximum density and that at the top of the principal cell is always comparable to the difference in density between that at the bottom of the cell and the maximum density. The largest motions in the stable portion of the layer are the horizontal motions at the top of the principal cell. The amplitude of these motions is a large fraction of the largest vertical velocity in the principal cell. Townsend (1964) observed horizontal motions in the lowest part of the stable region. The calculated results do not show any large vertical velocities in the stable region. Vertical motions in the stable region would require doing work against buoyancy forces. The essential energy balance is between energy released by buoyancy forces and viscous energy dissipated in the principal cell. The counter cells do not contribute significantly to the energy balance.

The behaviour of the system at very large Rayleigh number appears to approach one very slender principal cell with negligible or non-existent counter cells. However, caution must be used in interpreting the cell shape predicted at large Rayleigh numbers by the mean field approximation (see the discussion

by Deardorff & Willis 1965). Also the upper boundary could become important at high Rayleigh numbers.

At high Rayleigh numbers the effective Nusselt number can be described closely by

$$N_E = 1{\cdot}88 R_E^{\frac{1}{3}}. \tag{35}$$

A similar expression can be obtained at each λ relating the ordinary Nusselt number and the ordinary Rayleigh number (compare the upper right-hand portions of figures 4 and 7).

Comparison with experiment

The velocities in the ice-water problem are small and difficult to measure in the laboratory. It is more practical to measure temperatures. Two convenient quantities to compare with theoretical calculations are the mean temperature profile and the heat transport, both of which were measured by Townsend (1964). However, calculations discussed here employed for simplicity a free (slip) boundary at the bottom of the layer. For direct comparison with experiment it would be necessary to use a rigid (non-slip) lower boundary. The details of the upper boundary would probably not be important. The calculated mean temperature profile in figure 1 has the same effective Nusselt number as the measured profile; that is, the initial point, the initial slope and the point at 4 °C are the same for both curves. Agreement at other points in the unstable region is favourable. Agreement in the stable portion of the layer is not as favourable. The temperature distribution in the stable region is determined principally by conductive heat transport. The laboratory measurements indicate that a large fraction of the heat transported through the lower boundary must have entered the system through the sides of the apparatus and not through the upper boundary, while the calculations assume that all heat enters the system at the upper boundary. For this reason good agreement is not to be expected between the calculated and observed results in the stable region.

A rough comparison of the heat flux at a given Rayleigh number for the calculated and measured results can be obtained as follows: Herring (1963, 1964) derived expressions of the form of equation (35) for the heat flux in the ordinary parallel plate convection problem for both free and rigid boundaries. The proportionality constant is a factor of 2·7 times smaller for the rigid boundary case than for the free boundary case, since a rigid boundary restricts fluid motions more than a free boundary. If the introduction of a rigid lower boundary into the ice-water problem lowers the heat transport in (35) by the same factor, the effective Rayleigh number of 46,000 for the experimental case would lead to an effective Nusselt number of 25. This is 1·9 times the measured value of 13. This method probably overestimates the heat flux since the effect of introducing a rigid boundary into the ice-water problem is probably more important than in the ordinary parallel-plate convection problem, as the additional restriction to the motions is applied just at the point where the fluid is most buoyant.

Equations (24) and (25) were used to estimate the importance of the three neglected fluctuating interactions. All of the fluctuating interactions were much more important in the principal cell than in the counter cells. The ratio of

the root mean square average of a neglected fluctuating term to the root mean square average of the term retained in the same equation was taken as a measure of the importance of a particular fluctuating interaction. There is a general tendency for the importance of the fluctuating interactions to increase with increasing λ and R. The second term in equation (24) which can be related physically to turbulent momentum transport is generally a factor of at least ten less than the term retained. This results from the fact that this term is multiplied by the reciprocal of the Prandtl number, and the Prandtl number of water is 11·5 at 4 °C. The second term in equation (25), which can be associated physically with turbulent heat transport, is comparable with the term retained except at low λ and R. The Θ^2 term in equation (25) was the most troublesome, always within a factor two of the term retained, and was relatively insensitive to changes in λ and R. When this term is neglected, the buoyancy of the rising portion of a convective cell is equal to that of the descending portion. When this term is included, the buoyancy force is increased for the rising portion of the cell but decreased for the descending portion. For either the convective roll or the rectangular cell, this term does not modify the energy integral of the problem, so that this term appears to alter the nature of the buoyancy force but not the total amount. That the Θ^2 term is important may be seen from the case illustrated in figure 8, where most of the descending portion of the principal cell is slightly stable, so that the effect of including this term could make the descending portion of the cell actually work against the buoyancy force. Thus the energy to power the cell would have to come from the upward motion.

The mean field approximation forces the motions into a regular pattern of Bénard-like cells. This is a considerable idealization of the actual situation. Townsend (1964) interprets the variations of temperature in the unstable portion of the layer as caused by isolated rising convective elements, with no observed descending elements. This is probably related to the fact that the fluctuating term in the buoyancy, which was neglected in this investigation, destroys the symmetry between upward and downward motions. In addition, the largest temperature fluctuations in the laboratory were found just at the bottom of the stable region. Townsend (1964) interprets this in terms of internal gravity waves caused by rising convective elements running into the stable region. Also, internal gravity waves may be related to the oscillations which made convergence so cumbersome in this investigation. Finding steady-state solutions to this problem using the mean field approximation eliminates the possibility of obtaining any information about small-scale, time-dependent or turbulent phenomena.

Even though it was not possible to show formally that all terms neglected are small, agreement with experiment was favourable, in so far as comparison with experiment was possible. Herring (1964) also obtained favourable agreement with experiment using the mean field approximation for the ordinary parallel-plate convective problem. The mean field approximation should still give useful information about averaged properties of the ice-water system.

Summary of results

The solutions obtained show the following general properties of the ice-water system.

(i) Convective instability takes place at a finite amplitude.

(ii) Convective motions substantially alter the temperature structure of the layer.

(iii) When the temperature of the upper boundary is sufficiently high the upper boundary is not important dynamically.

(iv) The important penetration of convective motions into the stable region takes place in the form of nearly horizontal motions at the bottom of the stable region.

These general properties probably do not depend on the mean field approximation.

Comments by Dr W. V. R. Malkus, Dr C. Rooth and Dr G. Veronis were very helpful in this investigation. Mr Ira Kaskel produced the computer-drawn contour plots.

REFERENCES

DEARDORFF, J. W. & WILLIS, G. E. 1965 *J. Fluid Mech.* **23**, 337.

FOX, L. 1957 *The Numerical Solution of Two-point Boundary Problems in Ordinary Differential Equations.* Oxford: Clarendon Press.

FURUMOTO, A. & ROOTH, C. 1961 Notes of summer study program in geophysical fluid dynamics of the Woods Hole Oceanographic Institution (unpublished).

GLOBE, S. & DROPKIN, D. 1959 *J. Heat Transfer*, **81**, 24.

HENYEY, L. G., WILETS, L., BOHM, V. H., LELEVIER, R. & LEVEE, R. D. 1959 *Astrophys. J.* **129**, 628.

HERRING, J. R. 1963 *J. Atmos. Sci.* **30**, 325.

HERRING, J. R. 1964 *J. Atmos. Sci.* **21**, 277.

LEIGHTON, R. B. 1963 *Annual Review of Astronomy and Astrophysics*, p. 19. Palo Alto: Annual Reviews Inc.

MALKUS, W. V. R. 1960 *Aerodynamic Phenomena in Stellar Atmospheres*, p. 346. Bologna: Zanichelli.

MALKUS, W. V. R. & VERONIS, G. 1958 *J. Fluid Mech.* **4**, 225.

RAYLEIGH, J. S. 1916 *Phil. Mag.* **32**, 529.

SILVESTON, P. L. 1958 *Forsch. Gebiete Ingenieurn.* **24**, 59.

SIMPSON, J., SIMPSON, R. H., ANDREWS, D. & EATON, M. A. 1965 *Rev. Geophys.* **3**, 38.

TOWNSEND, A. A. 1964 *Q. J. Roy. Meteorol. Soc.* **90**, 248.

VERONIS, G. 1963 *Astrophys. J.* **137**, 641.

VERONIS, G. 1966 *J. Fluid Mech.* **24**, 545.